IEEE Access
Multidisciplinary | Rapid Review | Open Access Journal

Received February 1, 2018, accepted February 26, 2018, date of publication March 8, 2018, date of current version April 4, 2018.

Digital Object Identifier 10.1109/ACCESS.2018.2813987

Efficiency Optimization of PMSM Drives Using Field-Circuit Coupled FEM for EV/HEV Applications

JIANHUA WU[1], JING WANG[1], CHUN GAN[2], (Member, IEEE), QINGGUO SUN[1], AND WUBIN KONG[3], (Member, IEEE)

[1]College of Electrical Engineering, Zhejiang University, Hangzhou 310027, China
[2]Department of Electrical Engineering and Computer Science, The University of Tennessee, Knoxville, TN 37996, USA
[3]School of Electrical and Electronic Engineering, Huazhong University of Science and Technology, Wuhan 430074, China

Corresponding author: Chun Gan (cgan@utk.edu)

This work was supported by the Chinese National 863 Program under Grant 2011AA11A101.

ABSTRACT This paper proposes an efficiency optimization method for the permanent magnet synchronous motor (PMSM) based powertrain by using field-circuit coupled finite-element method (FEM) for electric vehicle or hybrid electric vehicle applications. In this paper, an alterable flux-weakening (FW) angle is employed in the armature current control strategy for the FW operation. The optimal FW angle for each certain operating condition can be obtained through the pre-selection, which improves the system efficiency compared to conventional FW methods. Then, the lookup table (LUT) for optimal armature current control commands is obtained. Through using this optimal LUT in the drive system, the system efficiency can be significantly improved for the entire operation range. The time-stepping FEM is used to simulate the PMSM system, which integrates the electromagnetic field analysis of the motor prototype and the control algorithm of the drive system. A 2-D transient FEM model is built for a 15 kW PMSM in ANSYS Maxwell, and a vector control circuit model is set up in ANSYS Simplorer. Experiments are carried out on the 15 kW PMSM prototype to verify the accuracy of the simulation results and the effectiveness of the proposed design method.

INDEX TERMS Efficiency optimization, field-circuit coupling, permanent magnet synchronous motor (PMSM), time-stepping finite-element method (FEM).

I. INTRODUCTION

Electrical machine drive systems are a key point for electric vehicle (EV) and hybrid electric vehicle (HEV) applications. Permanent magnet synchronous motor (PMSM) has been used as a propulsion motor in EVs due to their superiorities, such as high efficiency and high power density [1]–[9]. The wide-speed operation is required in EV/HEV applications, and thus the flux-weakening (FW) control should be adopted to expand the operating limits of PMSM.

The FW control of PMSM can be achieved by controlling the armature currents with feedforward methods based on the equation calculation, feedback regulation methods, and hybrid methods [10]–[23]. FW methods in previous literature mainly focus on the control performance, such as dynamic response and steady-state characteristics, while the system efficiency has not been investigated in detail. Usually, the system efficiency is not considered as a target in the design process of the control strategy. However, the efficiency is an important index for practical EV traction systems. Therefore, developing an accurate design method considering the system efficiency of the PMSM system for EVs is very important [24], [25]. In [26], an optimal lookup table (LUT) acquired by offline calculation is utilized in the overall power control strategy for the small-scale wind energy convention system. This LUT-based optimization method is an effective solution for optimal motor control strategy.

There are mainly three methods for motor system design, including the magnetic field analysis [21], circuit simulation [26], and field-circuit coupled method [27]–[32]. Accurate control algorithm modeling can be achieved in circuit simulation, while it is hard to analyze the inherent motor characteristics precisely. Accurate study on the motor performance can be achieved by magnetic field analysis, while it is unable to investigate the system performance under various

control strategies. These two methods cannot guarantee the analysis accuracy of the entire motor systems with independent using. However, the field-circuit coupled method integrates both of the electromagnetic field analysis for the motor and control algorithm of the driving system. Field-circuit coupled analysis implemented by time-stepping finite-element method (TS-FEM) has received much attention for motor systems. In [27], a time-stepping two-dimensional (2-D) eddy-current FEM is proposed to investigate the performance of skewed rotor induction machines. In [28], a field-circuit coupled TS-FEM is presented to simulate the electromagnetic characteristics of PMSMs in the self-starting and voltage/frequency control processes. In [29], a coupled-circuit TS-FEM is employed to analyze the performance of a stand-alone permanent magnet synchronous generator. In [30], a simulation method for the steady-state magnetic fields of blocking up for the induction motor is proposed. The field-circuit coupled model is combined with time-periodic FEM to reduce the simulation time. In [31], the TS-FEM is developed by using FORTRAN. In [32], the field-circuit coupled simulation model for switched reluctance motor system is designed by using ANSYS Maxwell and ANSYS Simplorer.

These studies have shown that the field-circuit coupled TS-FEM is a promising solution for the motor system analysis. Since the motor system is an electromechanical integration product combining the electrical machine, power electronics, and control algorithm, this paper adopts field-circuit coupled TS-FEM to analyze the entire PMSM drive system. With this method, the mutual coupling of the motor and the drive system with different control strategies can be analyzed. Thus, the motor system performance can be comprehensively assessed. However, the system efficiency of the PMSM drive system considering control strategies has not been investigated in detail in previous field-circuit coupled studies. Considering this point, this paper aims at developing an accurate and optimal design method for the PMSM system by taking both the control strategy and system efficiency into account. Space vector pulse width modulation (SVPWM) strategy is adopted in this method, which is not considered in the conventional method that directly sets sinusoidal current excitations.

In this paper, a design method considering overall efficiency optimization for PMSM systems is proposed for EV/HEV applications. An alterable FW angle is employed in the armature current control strategy, and the optimal FW angle for each certain operating condition can be obtained through pre-selection, which improves the system efficiency. Then, the optimal LUT for armature current control commands is obtained. By using this optimal LUT in the drive system, the system efficiency can be significantly improved for the entire operation range. Field-circuit coupled TS-FEM is employed to guarantee the analysis precision by integrating a 2-D transient electromagnetic field model for the PMSM in ANSYS Maxwell and a vector control circuit model in ANSYS Simplorer. The optimal LUT for current control is obtained by the coupled simulation under different operating conditions. Experiments are carried out on a 15 kW PMSM prototype for further validation. The simulation and experimental results show a good consistency, which verifies the effectiveness and accuracy of the proposed design method.

II. FLUX-WEAKENING OPERATION OF PMSM

A. PMSM SYSTEM

A PMSM drive system is mainly composed of a PMSM, a power converter, a drive circuit, a position detection circuit, and a current sampling circuit, as shown in Fig. 1. The PMSM is extremely appropriate for extended speed operation in the FW mode [2]. Since the permanent magnets (PMs) are buried inside the rotor iron, they are effectively shielded from the demagnetizing armature reaction field during FW operation. The V-shaped disposition of the PMs serves to increase the air gap flux.

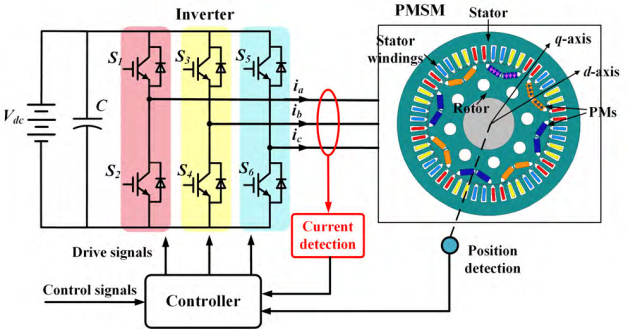

FIGURE 1. PMSM drive system.

In the d-q coordinate system, the steady-state voltage and torque equations of interior PMSM are expressed as follows:

$$\begin{bmatrix} u_d \\ u_q \end{bmatrix} = \begin{bmatrix} R & -\omega_e L_q \\ \omega_e L_d & R \end{bmatrix} \begin{bmatrix} i_d \\ i_q \end{bmatrix} + \begin{bmatrix} 0 \\ \omega_e \psi_f \end{bmatrix} \tag{1}$$

$$T_e = \frac{3}{2} P_n [\psi_f + (L_d - L_q) i_d] i_q \tag{2}$$

where u_d, u_q, i_d, i_q, L_d, L_q are the d- and q-axis components of armature voltage, current, and inductance, respectively; R, P_n, ψ_f, p are the armature resistance, number of pole pairs, permanent-magnet flux-linkage and the differential operator, respectively; T_e and ω_e are the electromagnetic torque and electrical angular velocity.

In the system, the armature current I_a and voltage U_a are limited as follows:

$$I_a = \sqrt{i_d^2 + i_q^2} \le I_{am} \tag{3}$$

$$U_a = \sqrt{u_d^2 + u_q^2} \le U_{am} \tag{4}$$

The current limit I_{am} is determined by the continuous armature current rating and available output current of the inverter. The voltage limit U_{am} is the maximum available output voltage depending on the dc-link voltage. When the SVPWM strategy is applied, the voltage limit is $U_{am} = V_{dc}/\sqrt{3}$.

B. FW METHODS

The PMSM control is divided into the maximum torque per ampere (MTPA) strategy in the constant torque region and FW strategy in the constant power region. Within the base speed range, the dc bus voltage of the inverter is sufficient to compensate the back EMF. Therefore, MTPA control can be applied to guarantee the minimum copper loss and generate maximum torque [33], [34]. However, when motor speed exceeds the base speed, MTPA control is not suitable for this condition. Hence, FW control strategy is adopted to achieve constant power operation.

Generally, feedforward or feedback FW methods are applied to the current controller. Feedforward methods are based on the mathematical model of the PMSM and utilize motor parameters and dc bus voltage to calculate the reference armature current vector. Typically, d- and q-axis current references can be derived from the current and voltage constraints in different speed regions. The principle of MTPA control in the constant torque region can be expressed as:

$$\frac{\partial \left(T_e/I_a\right)}{\partial i_d} = 0, \quad \frac{\partial \left(T_e/I_a\right)}{\partial i_q} = 0 \tag{5}$$

From (1) $\sim$ (5), i_d for MTPA control and FW control can be formulated as (6) and (7), respectively, and i_q can be obtained by (8).

$$i_d = \frac{-\psi_f + \sqrt{\psi_f^2 + 8(L_d - L_q)^2 I_a^2}}{4(L_d - L_q)} \tag{6}$$

$$i_d = \frac{-\psi_f L_d + \sqrt{(\psi_f L_d)^2 - (L_d^2 - L_q^2)[\psi_f^2 + L_q^2 I_a^2 - (\frac{U_{am}}{\omega_e})^2]}}{L_d^2 - L_q^2} \tag{7}$$

$$i_q = \sqrt{I_a^2 - i_d^2} \tag{8}$$

The armature resistance is usually neglected in the voltage equation to simplify the analytical solution [21]–[23]. The block diagram of a typical feedforward method is shown in Fig. 2(a). Below and above the base speed, the d-axis current reference is calculated by (6) and (7), respectively. The feedforward methods are sensitive to the motor parameters variation and operating conditions.

Feedback methods are generally based on the direct control of the inverter output voltage through a closed-loop regulation controller. Fig. 2(b) shows the block diagram of a typical feedback method. i_d is regulated by a proportional and integral (PI) compensator, which is fed by the error between the reference voltage vector and voltage limit. When SVPWM strategy is applied, the voltage limit is $k_s \cdot V_{dc}/\sqrt{3}$, where $k_s < 1$ is a safety factor. Since the motor parameters are not required, the control performance is more robust to motor parameter variations.

The feedforward and feedback FW methods are very useful, since they are universal to all PMSMs. But for a practical PMSM drive used in EV traction system, the optimal control performance cannot be obtained by these methods, because the parameter variation and efficiency consideration are often neglected in the control algorithm. In these methods, the current vector can not be adjusted to find the optimal efficincy operation. Besides, the calculation amount of the feedforward method is large, and the voltage feedback method may have problems in system stability and speed response.

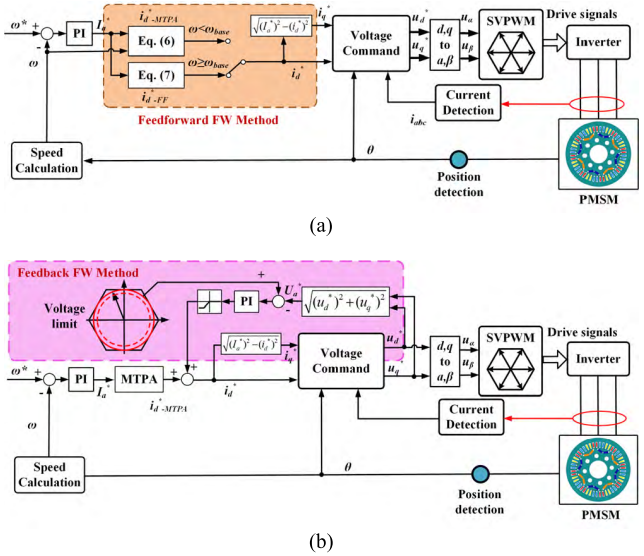

FIGURE 2. Typical FW methods. (a) Feedforward. (b) Feedback.

III. PROPOSED EFFICIENCY OPTIMIZATION METHOD USING FIELD-CIRCUIT COUPLED TS-FEM

A. PROPOSED EFFICIENCY OPTIMIZATION METHOD

In practical EV applications, LUT-based current control is usually employed for PMSMs. In this paper, an optimal LUT of armature current commands under different operating conditions is employed in the control algorithm to achieve efficiency optimization. The inputs of this LUT are the torque command and instantaneous motor speed, and the outputs are the d- and q- axis current commands. With this LUT, the optimal current commands for efficiency optimization can be stored in advance for a wide speed range.

The proposed efficiency optimization method is to find the corresponding optimal current command for different speeds and torques, so that the optimal current LUT can be obtained. To achieve this method, an alterable FW angle is introduced in the current control algorithm, and the FW control is implemented by adjusting the FW angle under different operating conditions. In this paper, the flux-weakening angle γ is defined as the angle between the armature current vector and the q-axis, as shown in Fig. 3.

i_d and i_q can be expressed as:

$$i_d = -\sqrt{2} I_a \sin\gamma, \quad i_q = \sqrt{2} I_a \cos\gamma \tag{9}$$

The demagnetizing current i_d increases when γ becomes larger, and the demagnetizing effect is more significant.

To obtain the LUT including the speed, torque, and current, a double closed-loop vector system for PMSM is employed.

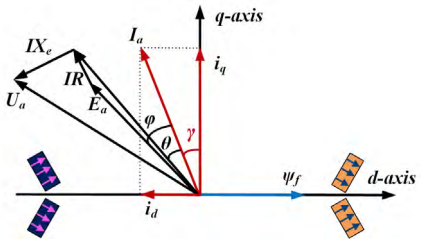

FIGURE 3. Vector diagram.

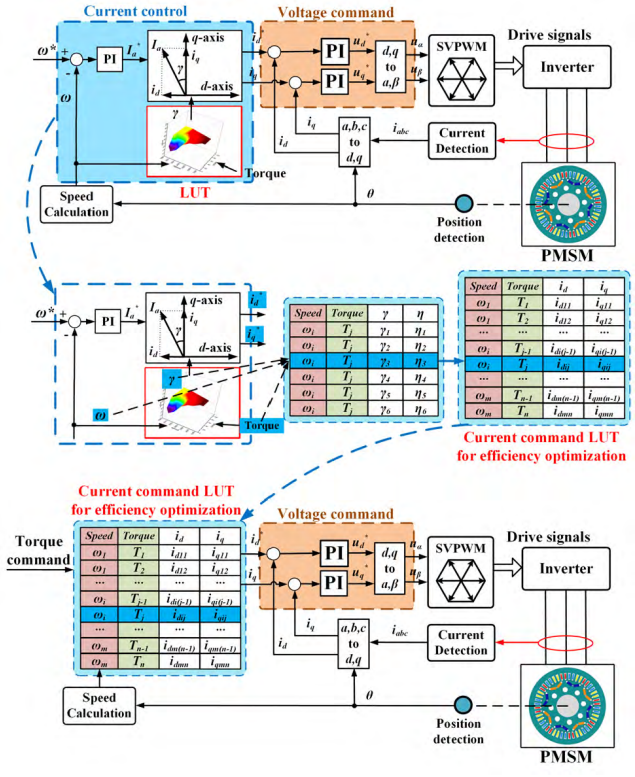

FIGURE 4. Proposed design method with efficiency optimization.

The block diagram of the control algorithm and the proposed design process is shown in Fig. 4.

In this PMSM system, the armature currents are not controlled by feedforward calculation or feedback compensation. Instead, an alterable FW angle is applied, where the system efficiency can be optimized accordingly. Different FW angles can be set to accommodate for different operating conditions. The optimal FW angles for each certain operating condition can be obtained through selection, which improves the system efficiency compared to conventional FW methods. Then the LUT with optimal armature current control commands is obtained, and the system efficiency optimization is achieved for the entire operation range.

The instantaneous speed is fed back to the PI controller, where the armature current command is obtained. The d- and q- axis armature current references are not determined by conventional feedforward or feedback methods, while determined by the output of the speed PI controller and an optimal LUT, where the FW angles for different operating conditions are stored. The d- and q- axis voltage references are obtained from the two current PI controllers. The voltage space vector for pulse width modulation is obtained by a coordinate transfer. After the space vector pulse width modulation, drive signals are generated for the power switches.

For a certain operating condition, when the reference speed, load torque, and FW angle are set, the steady-state d- and q- axis current commands for this operating condition can be then obtained, as shown in Fig. 4. The critical point is to judge whether the tested FW angle is the optimal one for this operating condition with the maximum system efficiency. After a range of FW angles are tested, the optimal angle can be selected. Then the system efficiency in this operating condition is improved by the optimal FW angle. Through adjusting the FW angle, the corresponding optimal control commands for this operating condition can be further obtained. By this way, the variation of the parameters such as inductances does not need to be considered in the control algorithm.

The design process of the current based LUT for motor system efficiency optimization is shown in Fig. 5. The LUT is obtained by the current commands in selected discrete operating conditions. Therefore, the design of the optimal control commands can be divided according to different speeds and torques. For a certain speed, the first step is to figure out the optimal FW angle on the contour line. Usually, this FW angle is the maximum angle for this speed. The second step is to determine the minimum angle with no load, which is usually the lower limit. The optimal FW angles for other operating conditions at this speed are between these two angles. After the current commands for all discrete speeds are determined, the optimal LUT for all operating conditions is obtained, and this improved LUT can be used in the PMSM drives to improve the system efficiency.

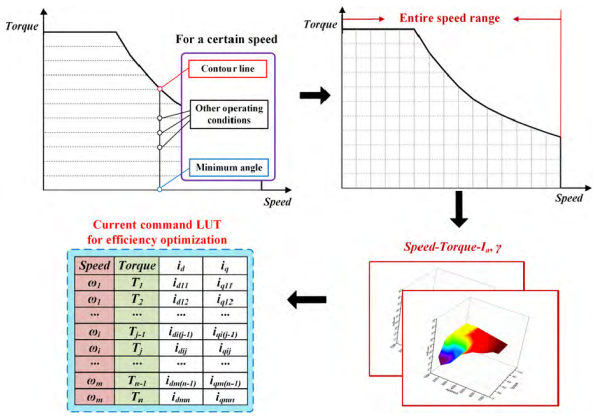

FIGURE 5. Design process of the current command LUT.

B. FIELD-CIRCUIT COUPLED ANALYSIS USING TS-FEM

The field-circuit coupled model can be obtained by coupling the 2-D magnetic field model and the exterior circuit model. The 2-D magnetic field equation of PMSM for

magnetic vector potential A is given by

$$\frac{\partial}{\partial x}\left(\frac{1}{\mu}\frac{\partial A}{\partial x}\right)+\frac{\partial}{\partial y}\left(\frac{1}{\mu}\frac{\partial A}{\partial y}\right)=-J \tag{10}$$

where x, y are the rectangular coordinates; μ is the permeability; J is the externally impressed current density.

When equation (10) in the field domain needs to be coupled with the external circuit, the circuit equation can be expressed as [27] and [28]:

$$U_s=R_s i_s+L_e\frac{di_s}{dt}+\frac{l_a}{s}\left(\iint_{\Omega_+}\frac{\partial A}{\partial t}d\Omega-\iint_{\Omega_-}\frac{\partial A}{\partial t}d\Omega\right) \tag{11}$$

where U_s is the stator phase voltage, R_s is the total stator resistance, L_e is the end winding inductance, l_a is the axial length of the iron core, s is the cross-section area of one turn, Ω_+ and Ω_- are the total areas of positively and negatively oriented coil sides of the phase winding in the solution sector, respectively.

Equations (10) and (11) constitute the field-circuit coupled equations. In this paper, the TS-FEM is employed to solve the field-circuit coupled problem, and develop the simulation model for the proposed efficiency optimization method.

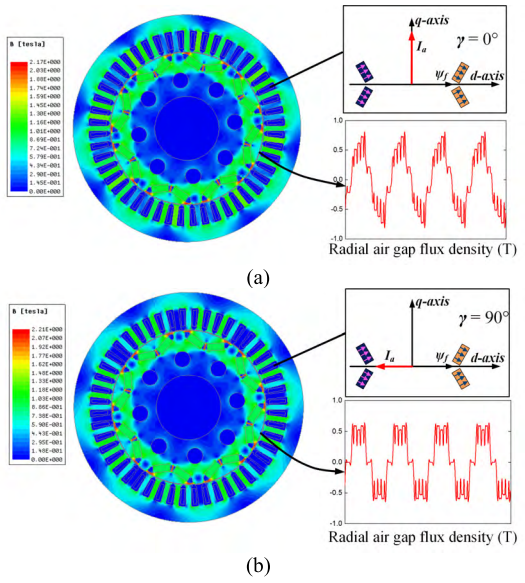

FIGURE 6. Magnetic flux density distribution. (a) $\gamma = 0°$. (b) $\gamma = 90°$.

This paper uses ANSYS software to implement the field-circuit coupled analysis based on TS-FEM. Fig. 6 shows the distributions of the magnetic flux density and the radial air gap flux density. The RMS value of three phase currents is set to 350 A, and the FW angles are set to 0° and 90°, respectively. It can be seen that the flux density at 90° FW angle is smaller than that at 0° FW angle, and the demagnetizing effect is more significant. It means that the demagnetization effect of the armature current is considered in the FEM analysis, which is an advantage compared to the circuit method.

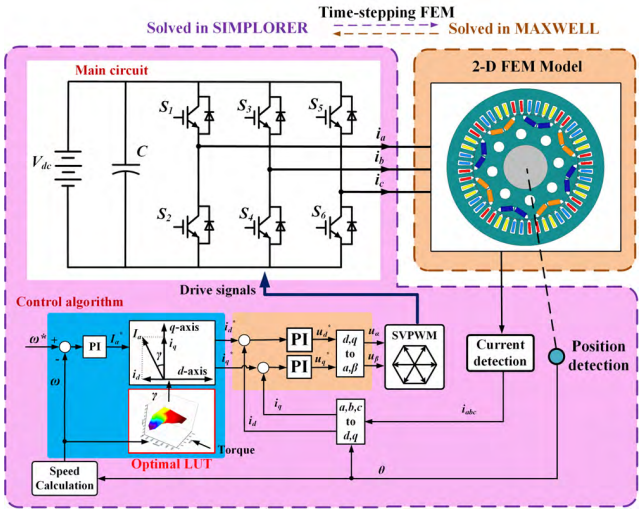

FIGURE 7. Proposed field-circuit coupled design method by using TS-FEM.

The exterior control circuit model of the PMSM system is set up in ANSYS Simplorer. The coupled simulation system can be developed by integrating the field model of the motor and the circuit model of the control algorithm, as shown in Fig. 7. The TS-FEM ensures the instantaneous values of the field and circuit variables to be solved simultaneously, and the armature inductances are naturally considered in the field analysis, which improves the simulation accuracy. By using the field-circuit coupled method, the efficiency optimization method based on the improved LUT is developed under different motor speeds, currents, and torques. The system efficiency can be calculated by

$$\eta=\frac{\omega_m\cdot T_l}{V_{dc}I_{dc}} \tag{12}$$

where η is the system efficiency, ω_m is the motor mechanical angular velocity, T_l is the load torque, V_{dc} and I_{dc} are the dc bus voltage and current, respectively.

According to the efficiency results, optimal FW angles and current commands can be obtained for different operating conditions, and thus the efficiency optimization of the PMSM drive system can be achieved.

IV. FIELD-CIRCUIT COUPLED SIMULATION RESULTS

The field-circuit coupled simulation using TS-FEM is carried out on a 15 kW interior PMSM, and the main parameters of the motor are shown in Table 1. The co-simulation system for the proposed design method is developed in ANSYS platform by the 2-D FEM model for the PMSM in Maxwell and the circuit model in Simplorer, as shown in Fig. 8. A three phase bridge inverter is built by using IGBT modules, as shown in Fig. 8(a). A, B, C represent for the ends of the three phase armature windings. The series resistor R is the winding resistance of each phase, and the series inductance L_e is the end winding leakage inductance. Fig. 8(b) shows the control algorithm, where the SVPWM strategy is employed. The rotational inertia is set in the mechanical part. Different

TABLE 1. Motor parameters.

Parameter	Value
Rated power (kW)	15
Maximum power (kW)	28
Maximum current (A)	350
Maximum torque (N·m)	110
Rated speed (r/min)	2250
Maximum speed (r/min)	7500
DC voltage (V)	120
Number of pole pairs	4
Number of stator slots	48
Core length (mm)	140
Stator outer diameter (mm)	160
Stator inner diameter (mm)	108
Rotor outer diameter (mm)	106.8
Rotor inner diameter (mm)	45
Remanece (T)	1.1 (@120 °C)

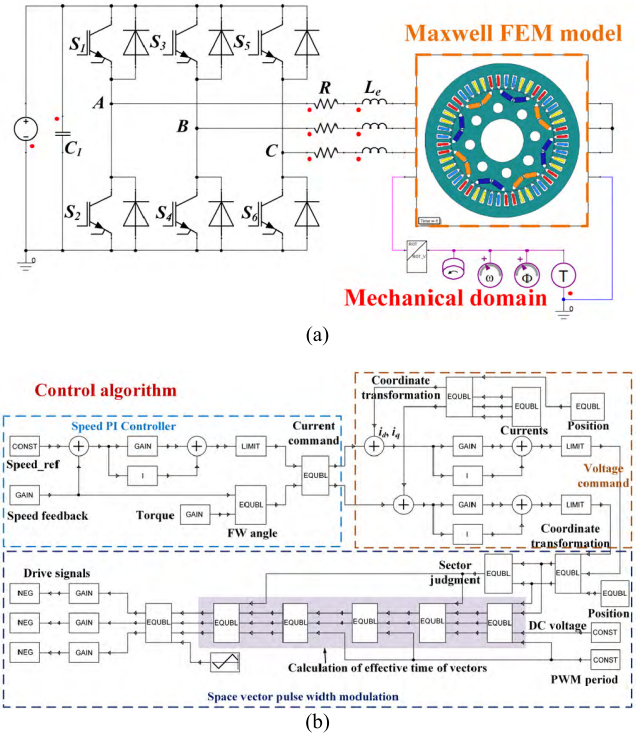

(a) (b)

FIGURE 8. Field-circuit coupled simulation model. (a) Main circuit. (b) Control algorithm.

speeds and torques are set to simulate various operating conditions.

The field-circuit coupled simulation is conducted at full speed range and different torque loads. In the constant torque region, the maximum torque is 110 N · m. In the constant power region, the maximum power is 28 kW. Different FW angles are set to test the system performance and efficiency. Then the optimal FW angles with the maximum system efficiency are selected for the current command LUT. Fig. 9 shows the steady-state current waveforms for some operating conditions on the contour line with optimal FW angles. The selected operating conditions are shown in Fig. 9(a). The waveforms of three phase armature currents

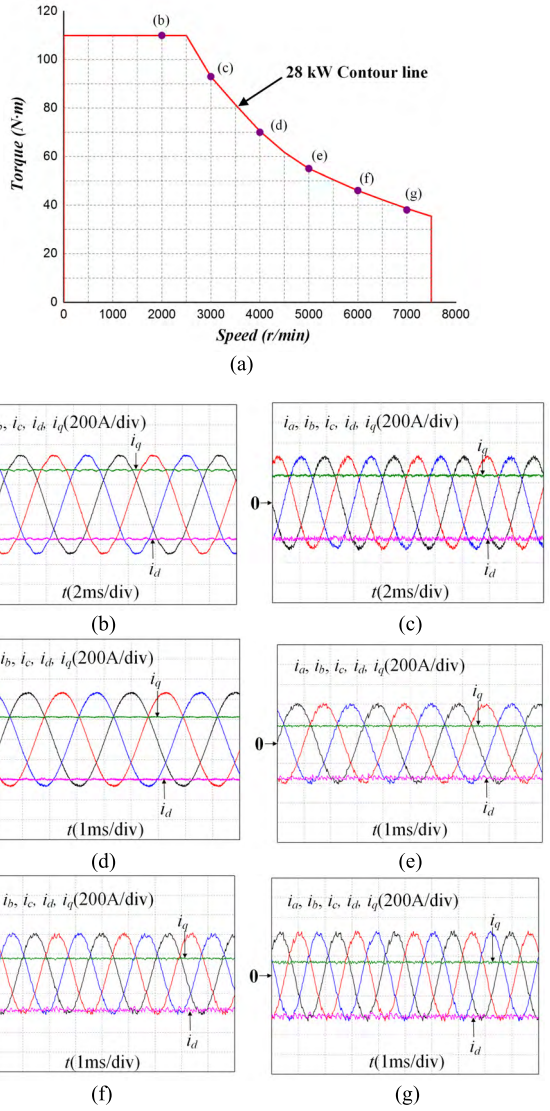

FIGURE 9. Steady-state currents at selected operating points. (a) Operating points. (b) 2000 r/min, 110 N · m, $\gamma = 45°$. (c) 3000 r/min, 90 N · m, $\gamma = 54°$. (d) 4000 r/min, 70 N · m, $\gamma = 60°$. (e) 5000 r/min, 54 N · m, $\gamma = 64°$. (f) 6000 r/min, 45 N · m, $\gamma = 68°$. (g) 7000 r/min, 38 N · m, $\gamma = 72°$.

i_a, i_b, i_c, and d- and q-axis currents i_d, i_q, are shown in Fig. 9(b)-(g). Fig. 9(b) shows the steady-state currents at 2000 r/min and 110 N · m load, where the FW angle is 45°. It can be seen that the steady-state values of i_d and i_q keep almost constant, which are 350 and -350 A, respectively. Similarly, Fig. 9(c)-(g) show the steady-state currents at 3000 r/min and 90 N · m, 4000 r/min and 70 N · m, 5000 r/min and 54 N · m, 6000 r/min and 45 N · m, and 7000 r/min and 38 N · m, when the FW angles are 54°, 60°, 64°, 68°, 72°, respectively.

V. EXPERIMENTAL VERIFICATION

In order to verify the effectiveness of the proposed field-circuit coupled design method based on TS-FEM, the experimental platform is set up on a 15 kW PMSM prototype, which

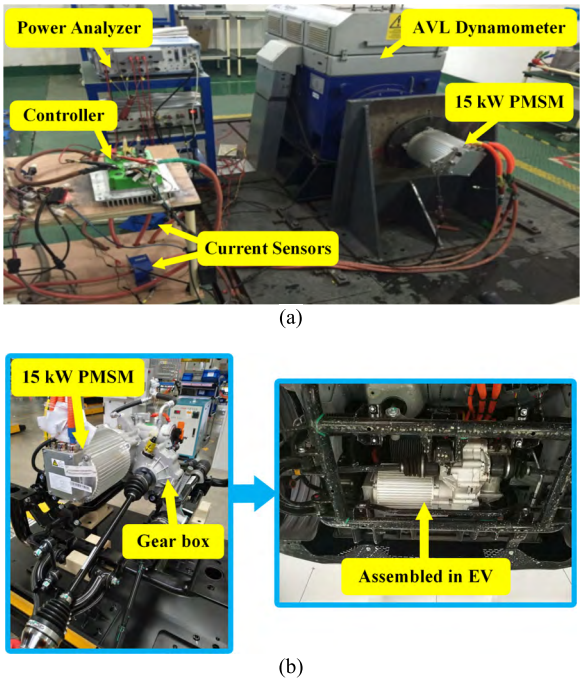

FIGURE 10. Experimental setup. (a) Off-board test. (b) On-board test.

is used for an EV traction drive, as shown in Fig. 10. The designed maximum speed of this EV is 100 km/h. Fig. 10(a) shows the off-board testbed. The experimental platform is mainly composed of the 15 kW PMSM, current sensors, a power analyzer, a controller and a dynamometer. A digital chip STM32F302VCT7 is employed to implement the control strategy and generate control signals to drive the PMSM. Current sensors LEM IT-700-S are used to detect the instantaneous current information for the controller. An AVL dynamometer INDY S22-2/0525-1BS-1 acts as the load, and thus the PMSM at different speeds and torques can be investigated. Power analyzer Yokogawa WT3000 is used to analyze the power and efficiency of the system. Fig. 10(b) shows the on-board test setup when the PMSM system is installed in an electric vehicle.

Fig. 11 shows the control diagram of the PMSM drive system by using the proposed method. The optimal current command LUT is employed to generate the current commands for different operating conditions according to the torque command. The inputs of this LUT are the torque command and instantaneous speed feedback, and the outputs are d- and q- axis current references. The current references and feedbacks are then input into two PI controllers, where the d- and q- axis voltage references are calculated. After the coordinate transformation, the voltage SVPWM strategy is implemented to generate the drive signals for the power switches. An encoder is used to detect the rotor position for speed calculation and coordinate transformation. Three current sensors are used to detect the phase currents for control.

Experiments are carried out at full speed range and different load torques. In the experiments, the optimal current

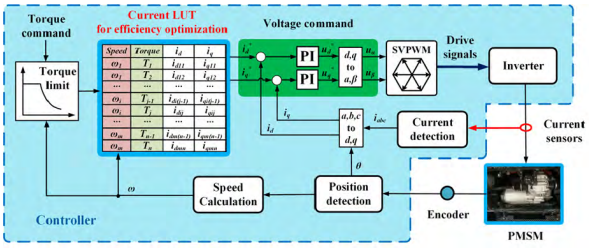

FIGURE 11. Control schematic by using the proposed method.

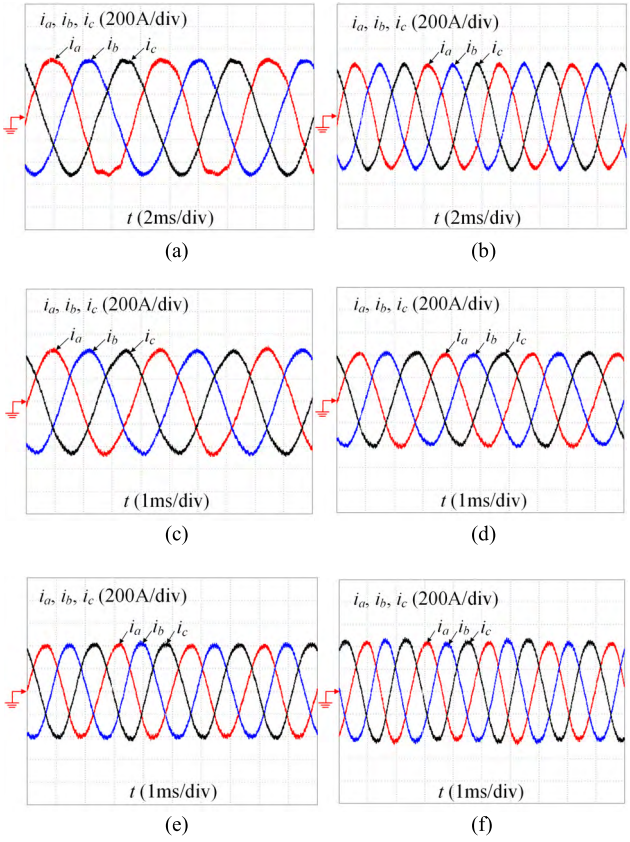

FIGURE 12. Steady-state currents. (a) 2000 r/min, 110 N · m. (b) 3000 r/min, 90 N · m. (c) 4000 r/min, 70 N · m. (d) 5000 r/min, 54 N · m. (e) 6000 r/min, 45 N · m. (f) 7000 r/min, 38 N · m.

command LUT is stored in the controller. Control signals are provided by the controller to drive the PMSM, and the load torque is implemented by the dynamometer. Then the PMSM operating at different given speeds and torque loads can be achieved through adjusting the control parameters. When the PMSM achieves steady state, current waveforms are recorded, and the power and efficiency of the system are analyzed by the power analyzer. In the constant torque region, the maximum torque is 110 N · m; in the constant power region, the maximum power is 28 kW. Fig. 12 shows the measured steady-state waveforms of the three phase armature currents. Fig. 12 (a)-(g) show the currents under the same operating conditions as in the simulation, presenting a good consistency.

Fig. 13(a) shows the comparison between the measured and simulated system efficiency and bus current at different

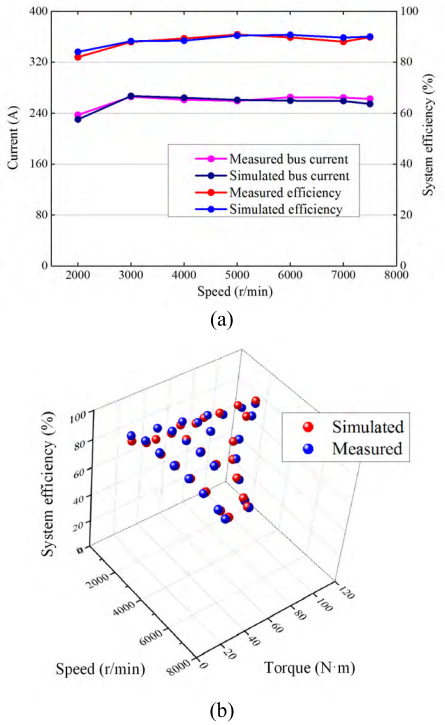

FIGURE 13. Comparison between simulated and measured results. (a) Efficiency and bus current on the contour line. (b) Efficiency over wide operation range.

operating points on the contour line. It can be seen that both the bus current and efficiency results match well. Fig. 13(b) shows the system efficiency comparison over a wide speed range at different torque loads. Clearly, the difference between the simulated and measured system efficiency is less than 2%, which ensures the accuracy of the designed field-circuit coupled simulation.

The efficiency results over entire operation range are collected to draw the efficiency contour map of the PMSM system, as shown in Fig. 14. Fig. 14(a) shows the simulated efficiency contour map based on the field-circuit coupled TS-FEM; Fig. 14(b) shows the measured system efficiency map. The two maps show a good agreement over the entire operation range. Although the system efficiency is low at low speed and large torque region, the system efficiency is relatively high in the high speed FW operation area.

To verify the effectiveness of the proposed efficiency optimization method, experiments are also carried out with conventional feedforward FW method. The comparison of the system efficiency at rated power 15 kW and maximum power 28 kW is shown in Fig. 15. It can be seen that, in the conventional method, the efficiency results are not optimal, because it does not take the system efficiency into account in the calculation of current commands. However, the system efficiency by using the proposed efficiency optimization method is obviously higher than that of the conventional FW method. In some working conditions, more than 5% efficiency improvement can be achieved.

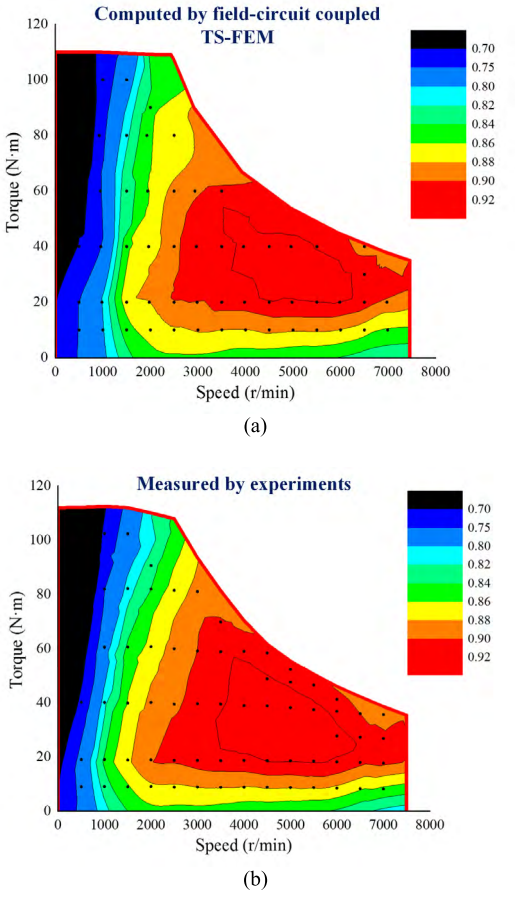

FIGURE 14. Comparison of system efficiency contour maps. (a) Computed by field-circuit coupled TS-FEM. (b) Measured by experiments.

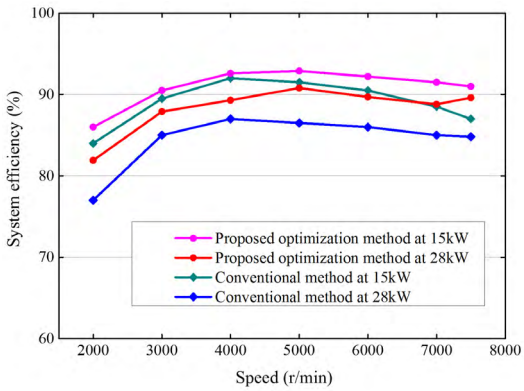

FIGURE 15. Efficiency comparison of proposed and conventional methods.

The effectiveness of the field-circuit coupled design method using TS-FEM has been verified by the experimental results. When the optimal current command LUT is employed in the control algorithm, the system efficiency is effectively optimized. It can be seen that sufficient agreement has been achieved between the simulated and the experimental results, confirming that the proposed field-circuit coupled design method has extremely high precision, which

can completely satisfy the precision requirements of the high-efficiency PMSM system design. The proposed method can be applied in the current control LUT design for high-efficiency EV/HEV applications.

VI. CONCLUSION

This paper proposes a design method for PMSM traction systems considering efficiency optimization by using field-circuit coupled FEM for EV/HEV applications. An alterable current FW angle is employed to improve the system efficiency. With the optimization of the FW angles, optimal current commands can be obtained for the current control LUT. The field-circuit coupled simulation system is developed by coupling the 2-D electromagnetic field model of the PMSM in ANSYS Maxwell and the control circuit model in ANSYS Simplorer. Experiments on a 15 kW EV-used PMSM are carried out to verify the accuracy of the simulation results and effectiveness of the proposed method. The system efficiency can be improved by 5% by using the proposed scheme compared to conventional methods.

The main contributions of this paper are as follows. First, an alterable flux-weakening angle through the pre-selection is employed for the flux-weakening operation of PMSM. Second, the field-circuit coupled time-stepping finite-element method is employed to design the current LUT for the PMSM drive, which can achieve a more accurate analysis. SVPWM strategy is adopted in this method, which makes the current waveforms more consistent with practical PMSM control than the conventional method that directly sets perfect sinusoidal current excitations. Third, a LUT-based overall efficiency optimization method is proposed for PMSM drives for EV/HEV applications, which can significantly improve the system efficiency. The proposed field-circuit coupled design method helps to improve the development process of the current control LUT for PMSM systems.

REFERENCES

[1] M.-S. Lim, S.-H. Chai, and J.-P. Hong, "Design of saliency-based sensorless-controlled IPMSM with concentrated winding for EV traction," *IEEE Trans. Magn.*, vol. 52, no. 3, Mar. 2016, Art. no. 820050.

[2] Z. Q. Zhu and D. Howe, "Electrical machines and drives for electric, hybrid, and fuel cell vehicles," *Proc. IEEE*, vol. 95, no. 4, pp. 746–765, Apr. 2007.

[3] K. T. Chau, C. C. Chan, and C. Liu, "Overview of permanent-magnet brushless drives for electric and hybrid electric vehicles," *IEEE Trans. Ind. Electron.*, vol. 55, no. 6, pp. 2246–2257, Jun. 2008.

[4] H.-C. Jung, G.-J. Park, D.-J. Kim, and S.-Y. Jung, "Optimal design and validation of IPMSM for maximum efficiency distribution compatible to energy consumption areas of HD-EV," *IEEE Trans. Magn.*, vol. 53, no. 6, Jun. 2017, Art. no. 8201904.

[5] S.-C. Carpiuc, "Rotor temperature detection in permanent magnet synchronous machine-based automotive electric traction drives," *IEEE Trans. Power Electron.*, vol. 32, no. 3, pp. 2090–2097, Mar. 2017.

[6] J.-M. Mun, G.-J. Park, S. Seo, D.-W. Kim, Y.-J. Kim, and S.-Y. Jung, "Design characteristics of IPMSM with wide constant power speed range for EV traction," *IEEE Trans. Magn.*, vol. 53, no. 6, Jun. 2017, Art. no. 8105104.

[7] M.-S. Lim, S.-H. Chai, and J.-P. Hong, "Design of saliency-based sensorless-controlled IPMSM with concentrated winding for EV traction," *IEEE Trans. Magn.*, vol. 52, no. 3, Mar. 2016, Art. no. 8200504.

[8] K. C. Kim, "A novel calculation method on the current information of vector inverter for interior permanent magnet synchronous motor for electric vehicle," *IEEE Trans. Mag.*, vol. 50, no. 2, pp. 829–832, Feb. 2014.

[9] P. B. Reddy, A. M. El-Refaie, K. K. Huh, J. K. Tangudu, and T. M. Jahns, "Comparison of interior and surface PM machines equipped with fractional-slot concentrated windings for hybrid traction applications," *IEEE Trans. Energy Convers.*, vol. 27, no. 3, pp. 593–602, Sep. 2012.

[10] S. Morimoto, M. Sanada, and Y. Takeda, "Wide-speed operation of interior permanent magnet synchronous motors with high-performance current regulator," *IEEE Trans. Ind. Appl.*, vol. 30, no. 4, pp. 920–926, Jul. 1994.

[11] J.-H. Song, J.-M. Kim, and S.-K. Sul, "A new robust SPMSM control to parameter variations in flux weakening region," in *Proc. IEEE Ind. Electron. Soc. Annu. Conf.*, Aug. 1996, pp. 1193–1198.

[12] J.-M. Kim and S.-K. Sul, "Speed control of interior permanent magnet synchronous motor drive for the flux weakening operation," *IEEE Trans. Ind. Appl.*, vol. 33, no. 1, pp. 43–48, Jan. 1997.

[13] M. N. Uddin, T. S. Radwan, and M. A. Rahman, "Performance of interior permanent magnet motor drive over wide speed range," *IEEE Trans. Energy Convers.*, vol. 17, no. 1, pp. 79–84, Mar. 2002.

[14] M. N. Uddin and M. M. I. Chy, "Online parameter-estimation-based speed control of PM AC motor drive in flux-weakening region," *IEEE Trans. Ind. Appl.*, vol. 44, no. 5, pp. 1486–1494, Sep. 2008.

[15] T. S. Kwon, G. Y. Choi, M. S. Kwak, and S. K. Sul, "Novel flux-weakening control of an IPMSM for quasi-six-step operation," *IEEE Trans. Ind. Appl.*, vol. 44, no. 6, pp. 1722–1731, Nov. 2008.

[16] T. S. Kwon, S. K. Sul, L. Alberti, and N. Bianchi, "Design and control of an axial-flux machine for a wide flux-weakening operation region," *IEEE Trans. Ind. Appl.*, vol. 45, no. 4, pp. 1258–1266, Jul. 2009.

[17] M. Tursini, E. Chiricozzi, and R. Petrella, "Feedforward flux-weakening control of surface-mounted permanent-magnet synchronous motors accounting for resistive voltage drop," *IEEE Trans. Ind. Electron.*, vol. 57, no. 1, pp. 440–448, Jan. 2010.

[18] H. Liu, Z. Q. Zhu, E. Mohamed, Y. Fu, and X. Qi, "Flux-weakening control of nonsalient pole PMSM having large winding inductance, accounting for resistive voltage drop and inverter nonlinearities," *IEEE Trans. Power Electron.*, vol. 27, no. 2, pp. 942–952, Feb. 2012.

[19] Y. Inoue, S. Morimoto, and M. Sanada, "Comparative study of PMSM drive systems based on current control and direct torque control in flux-weakening control region," *IEEE Trans. Ind. Appl.*, vol. 48, no. 6, pp. 2382–2389, Nov./Dec. 2012.

[20] S. Bolognani, S. Calligaro, and R. Petrella, "Adaptive flux-weakening controller for interior permanent magnet synchronous motor drives," *IEEE J. Emerg. Sel. Topics Power Electron.*, vol. 2, no. 2, pp. 236–248, Jun. 2014.

[21] K.-C. Kim, "A novel magnetic flux weakening method of permanent magnet synchronous motor for electric vehicles," *IEEE Trans. Magn.*, vol. 48, no. 11, pp. 4042–4045, Nov. 2012.

[22] D. Stojan, D. Drevensek, Z. Plantic, B. Grcar, and G. Stumberger, "Novel field-weakening control scheme for permanent-magnet synchronous machines based on voltage angle control," *IEEE Trans. Ind. Appl.*, vol. 48, no. 6, pp. 2390–2401, Nov./Dec. 2012.

[23] J. Lemmens, P. Vanassche, and J. Driesen, "PMSM drive current and voltage limiting as a constraint optimal control problem," *IEEE J. Emerg. Sel. Topics Power Electron.*, vol. 3, no. 2, pp. 326–338, Jun. 2015.

[24] X. Hu, J. Jiang, B. Egardt, and D. Cao, "Advanced power-source integration in hybrid electric vehicles: Multicriteria optimization approach," *IEEE Trans. Ind. Electron.*, vol. 62, no. 12, pp. 7847–7858, Dec. 2015.

[25] T. Liu, X. Hu, S. E. Li, and D. Cao, "Reinforcement learning optimized look-ahead energy management of a parallel hybrid electric vehicle," *IEEE/ASME Trans. Mechatronics*, vol. 22, no. 4, pp. 1497–1507, Aug. 2017.

[26] A. Shafiei, B. M. Dehkordi, S. Farhangi, and A. Kiyoumarsi, "Overall power control strategy for small-scale WECS incorporating flux weakening operation," *IET Renew. Power Generat.*, vol. 10, no. 9, pp. 1264–1277 Oct. 2016.

[27] S. L. Ho and W. N. Fu, "A comprehensive approach to the solution of direct-coupled multislice model of skewed rotor induction motors using time-stepping eddy-current finite element method," *IEEE Trans. Magn.*, vol. 33, no. 3, pp. 2265–2273, May 1997.

[28] M. A. Jabbar, Z. Liu, and J. Dong, "Time-stepping finite-element analysis for the dynamic performance of a permanent magnet synchronous motor," *IEEE Trans. Magn.*, vol. 39, no. 5, pp. 2621–2623, Sep. 2003.

[29] T. F. Chan, L. L. Lai, and L.-T. Yan, "Analysis of a stand-alone permanent-magnet synchronous generator using a time-stepping coupled field-circuit method," *IEE Proc.-Electr. Power Appl.*, vol. 152, no. 6, pp. 1459–1467, Nov. 2005.
[30] X. Wang and D. Xie, "Analysis of induction motor using field-circuit coupled time-periodic finite element method taking account of hysteresis," *IEEE Trans. Magn.*, vol. 45, no. 3, pp. 1740–1743, Mar. 2009.
[31] Y. Huangfu, S. Wang, J. Qiu, H. Zhang, G. Wang, and J. Zhu, "Transient performance analysis of induction motor using field-circuit coupled finite-element method," *IEEE Trans. Magn.*, vol. 50, no. 2, pp. 873–876, Feb. 2014.
[32] C. Gan, J. Wu, L. Zhang, S. Yang, and H. Wang, "Design and analysis on switched reluctance motor system using field-circuit coupled method," in *Proc. Int. Conf. Electr. Mach. Syst. (ICEMS)*, Oct. 2014, pp. 3296–3301.
[33] S. Bolognani, R. Petrella, A. Prearo, and L. Sgarbossa, "Automatic tracking of MTPA trajectory in IPM motor drives based on AC current injection," *IEEE Trans. Ind. Appl.*, vol. 47, no. 1, pp. 105–114, Jan./Feb. 2011.
[34] S. Kim, Y.-D. Yoon, S.-K. Sul, and K. Ide, "Maximum torque per ampere (MTPA) control of an IPM machine based on signal injection considering inductance saturation," *IEEE Trans. Power Electron.*, vol. 28, no. 1, pp. 488–497, Jan. 2013.

JIANHUA WU received the B.S. degree from the Nanjing University of Aeronautics and Astronautics, China, in 1983, and the M.S. and Ph.D. degrees from the Huazhong University of Science and Technology, China, 1991 and 1994, respectively, all in electrical engineering.

From 1983 to 1989, he was with Guiyang Electric Company as a Design Engineer. Since 2005, he has been a Professor with the College of Electrical Engineering, Zhejiang University, China. He developed the motor design software Visual EMCAD, which is widely used in China. His research interests are electric machine design and drives, including switched reluctance motors and permanent magnet machines for electric vehicle applications.

Dr. Wu is serving as the member of the Electrical Steel of Chinese Society for Metals, the Small-Power Machine Committee of China Electrotechnical Society, and the Standardization Administration of China.

JING WANG received the B.S. degree in electrical engineering from Zhejiang University, Hangzhou, China, in 2015, where he is currently pursuing the M.S. degree with the College of Electrical Engineering.

His research interests include control strategies of permanent magnet synchronous motor, especially for electric vehicle applications.

CHUN GAN (S'14–M'16) received the B.S. and M.S. degrees in power electronics and motor drives from the China University of Mining and Technology, Jiangsu, China, in 2009 and 2012, respectively, and the Ph.D. degree in power electronics and motor drives from Zhejiang University, Hangzhou, China, in 2016.

He is currently a Research Associate with the Department of Electrical Engineering and Computer Science, The University of Tennessee, Knoxville, TN, USA. He is also a Research Staff of the U.S. Energy/National Science Foundation cofunded Engineering Research Center CURENT. He has published over 50 technical papers in leading journals and conference proceedings, including over 20 IEEE Transaction papers, and authored one book chapter. He has 12 issued/published invention patents. His research interests include high-efficiency power converters, electric vehicles, electrical motor drives, electrical motor design, continuous variable series reactors, high-voltage direct current transmission, and microgrids.

Dr. Gan was a recipient of the 2018 Marie Sklodowska-Curie Actions Seal of Excellence from European Commission, the 2015 Top Ten Excellent Scholar Award, the 2016 Excellent Ph.D. Graduate Award, the 2015 Ph.D. National Scholarship, the 2015 Wang Guosong Scholarship, and the 2014 and 2015 Outstanding Ph.D. Candidate Awards in Zhejiang University.

QINGGUO SUN received the B.S. degree in electrical engineering from Qingdao University, Shandong, China, in 2014. He is currently pursuing the Ph.D. degree with the College of Electrical Engineering, Zhejiang University, Hangzhou, China.

His research interests include motor design and control in switched reluctance motor, particularly for the optimization of the torque ripple and efficiency of the motor system.

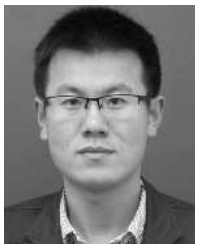

WUBIN KONG (M'15) was born in Zhejiang, China, in 1986. He received the B.S. and Ph.D. degrees from Zhejiang University, Hangzhou, China, in 2009 and 2014, respectively. His research interests are high-power multiphase motor drives and fault tolerant control motor drive applied in EV. Since 2015, he has been a Lecturer with the Huazhong University of Science and Technology, Wuhan, China.